



Description of the plasma delay effect in silicon detectors

Z. Sosin

Institute of Physics, Jagiellonian University in Krakow, Poland

ARTICLE INFO

Article history:

Received 14 February 2012

Received in revised form

3 July 2012

Accepted 9 July 2012

Available online 22 July 2012

Keywords:

Plasma delay

Current pulse

Pulse shape analysis

Particles identification

Silicon detector

ABSTRACT

A new method of modeling of the current signal induced by charged particle in silicon detectors is presented. The approach is based on the Ramo–Shockley theorem for which the charge carrier velocities are determined by taking into account not only the external electric field generated by the electrodes but also the Coulomb interaction between the electron and hole clouds as well as their diffusion.

© 2012 Elsevier B.V. All rights reserved.

1. Introduction

It is obvious that identification of particles and fragments produced in nuclear reactions is crucial for any experimental or technical work in nuclear physics. Among different ways of identifying charged particles the classical ΔE – E telescope method remains still the flagship. Recently, an alternative method based on the pulse shape discrimination (PSD) technique applied for silicon detectors is being developed and is increasingly drawing attention. Recent results demonstrate that the method can offer charge and isotopic identification comparable to that obtained with the classical ΔE – E method. The main advantage of the PSD method comes from the fact that it requires only one electronic channel for detection and identification. It is thus an important point for designing and constructing multi-detector systems.

A significant difference between the ΔE – E and the PSD techniques results from the fact that the former is governed basically by the energy loss process (Bragg curve), while the latter is primarily related to the plasma delay effect (PDE) [1–8]. In silicon detectors, this effect manifests itself with shortening of the pulse rise time with decreasing Z for low and intermediate mass fragments, for which the generated charge is practically completely collected by the detector electrodes. The experimental data demonstrate that the PDE concerns particles with small Z , for which the pulse height defect (PHD) is still of little importance.

For better understanding of the identification idea associated with PSD technique, and for its future development, it is crucial to have at ones command a perfect simulation of the time

dependence of the experimental signal produced by an ion with a given charge, Z , atomic mass, A , and energy, E . The main goal of such a simulation is to describe the extraction and collection of the generated charge carriers moving in the external electric field distorted due to the presence of a highly ionized track and due to the diffusion process of the carriers.

As presented in Ref. [9], an approach in which the distortion of the electric field caused by the generated carriers is neglected and is able to correctly describe the current signals for light charged particles (LCP), e.g. protons. However, this simplified approach completely fails in the case of heavy ions (HI) for which the collection time of the generated carriers gets longer ($\tau^{HI} > \tau^{LCP}$). Historically, this difference, associated to a slower carrier collection for HI, was quantified as a plasma delay (PD) effect. Since this effect influences the current signal rise-time, it appears to be crucial for the PSD technique.

An attempt to describe phenomenologically the delayed carrier collection time in silicon detectors has been recently proposed in Ref. [11]. The proposed description took into account the polarization of the electron–hole pairs generated by the HI and connected it to the relative dielectric permittivity. Another important assumption in cited paper was that the dissociation of pairs in time occurred with a constant probability and the modified electric field, inside and outside of the ion range, was given by the Maxwell equation for the electric field in the inhomogeneous medium. With these assumptions, the model was indeed able to describe the experimental pulse shapes quite accurately.

The presented way of modeling of a current pulse is quasi-microscopic and in some respect similar to that shown in Ref. [10]. One of the common features is a concept of clusters used

E-mail address: ufsosin@cyf-kr.edu.pl

instead of individual electrons and holes. In order to describe the motion of the center of mass of the cluster, we also take into account the mutual interactions among charge clouds (clusters). However, in contrast to Ref. [10], our approach does not limit the evolution of the cluster variance to the diffusion process alone, but also takes into account the drift in the electric field. Another important difference is related to the number of clusters considered and to the assumption of their shape. In our approach we are not limited to a finite number of clusters and we assume a continuous distribution of clusters of a Gaussian shape. Assuming the Gaussian shapes of the clusters we let the diffusion process to determine their nature.

On the other hand, an infinite number of clusters means that we are considering a continuous distribution of charge (which is not quantized). So we can say that in our approach, we describe the evolution of the distribution of charge density using a superposition of the Gauss functions.

In summary one can say, the main assumptions of the presented model are the following:

- i. Propagation of the electric charges (electrons, holes) generated in the detector is represented by evolution of the Gaussian clouds for which the centroids and variances are treated as independent variables.
- ii. Position of the centroid of each Gaussian is governed by the drift process, while its variance undergoes both diffusion and the drift process.

The first results of the model calculations indicate some attractive forces effects between the holes and electrons, in a region similar to that predicted by the phenomenological model of Ref. [11]. In this region also the electric field shows similar behavior to that presented in Ref. [11].

The detailed description of the new model is presented in the following section. The preliminary results of the calculations and comparison to the experimental data are presented in Section 3. Conclusions and possible extensions of the model applicability are given in Section 4.

2. Description of the model

A particle entering the silicon detector is assumed to degrade its energy according to the Bragg curve which relates the generated ionization $B(x)$ to the particle position x . We assume that the X -direction is perpendicular to the detector surface. In order to describe the initial, local, density of the electrons $\rho_e(\mathbf{r}, t=0)$ and holes $\rho_h(\mathbf{r}, t=0)$ we assume that the ionization is proportional to the energy loss at given position $B(x) = (1/w)(dE/dx)(x)$, where $w=3.62$ eV is the energy for an electron-hole pair production and $(dE/dx)(x)$ is the energy loss at given position (stopping power) [12]. Just after stopping of the impinging ion, the carrier density can be described as

$$\rho_e(\mathbf{r}, t=0) = -\rho_h(\mathbf{r}, t=0) = - \int B(x') \delta(x-x') \delta(y) \delta(z) dx' \quad (1)$$

where $\mathbf{r} = [x, y, z]$. This assumption states that for $t=0$ the ionization is localized along the X -axis only and disappears elsewhere.

In order to describe the time evolution of the generated ionization we assume its distribution in the following form:

$$\rho_e(\mathbf{r}, t) = \int B_e(x', t) G_e(x-x', y, z, t) dx' \quad (2)$$

$$\rho_h(\mathbf{r}, t) = \int B_h(x', t) G_h(x-x', y, z, t) dx' \quad (3)$$

which is analog to Eq. (1) and we set

$$-B_e(x, t=0) = B_h(x, t=0) = B(x) \quad (4)$$

Functions G_e and G_h are assumed to be Gaussians

$$G_e(x-x', y, z, t) = \frac{1}{\sqrt{(2\pi)^3 \sigma_e^2(x, t)}} \exp\left(-\frac{(x-x')^2 + y^2 + z^2}{2\sigma_e^2(x, t)}\right) \quad (5)$$

and

$$G_h(x-x', y, z, t) = \frac{1}{\sqrt{(2\pi)^3 \sigma_h^2(x, t)}} \exp\left(-\frac{(x-x')^2 + y^2 + z^2}{2\sigma_h^2(x, t)}\right). \quad (6)$$

If $\sigma_e \rightarrow 0$ and $\sigma_h \rightarrow 0$ for $t \rightarrow 0$ then the functions G_e and G_h can be regarded as representations of the δ function, thus

$$G_e(x-x', y, z, t=0) = G_h(x-x', y, z, t=0) = \delta(x-x') \delta(y) \delta(z) dx. \quad (7)$$

Now, the goal is to describe the time evolution of the functions B_e , B_h and G_e , G_h (for determination of G_e , G_h it is sufficient to derive the time evolution of their variances σ_e^2 and σ_h^2). In order to do it we define the one-dimensional densities associated with the variable x as

$$\eta_e(x, t) = \int_{-\infty}^{\infty} dy \int_{-\infty}^{\infty} dz \rho_e(\mathbf{r}, t) \quad (8)$$

$$\eta_h(x, t) = \int_{-\infty}^{\infty} dy \int_{-\infty}^{\infty} dz \rho_h(\mathbf{r}, t) \quad (9)$$

and we divide the thickness of the detector d_{Si} into N intervals $\Delta x = d_{Si}/N$. Let us assume that in the interval Δx_i ($i=1, N$) the associated values of σ_{ei} and σ_{hi} do not change substantially within the radius of a few sigma around Δx_i , and that a linear approximation can be used for the functions $B_e(x', t)$ and $B_h(x', t)$ within Δx_i

$$B_e(x', t) = p_{ei}(t)x' + q_{ei}(t) \quad (10)$$

$$B_h(x', t) = p_{hi}(t)x' + q_{hi}(t) \quad (11)$$

where $p_{ei} = (dB_e(x=x_i, t))/dx$ and $q_{ei} = B_e(x_i, t) - p_{ei}x_i$, and analogically $p_{hi} = (dB_h(x=x_i, t))/dx$ and $q_{hi} = B_h(x_i, t) - p_{hi}x_i$, and x_i means the centroid of interval Δx_i .

With the above assumption for x dependence, within an interval Δx_i one can approximate the densities

$$\eta_e(x, t) \approx \int_{-\infty}^{\infty} dx' \int_{-\infty}^{\infty} dy \int_{-\infty}^{\infty} dz (p_{ei}(t)x' + q_{ei}(t)) G_e(x-x', y, z, t) = p_{ei}(t)x + q_{ei}(t) \quad (12)$$

$$\eta_h(x, t) \approx \int_{-\infty}^{\infty} dx' \int_{-\infty}^{\infty} dy \int_{-\infty}^{\infty} dz (p_{hi}(t)x' + q_{hi}(t)) G_h(x-x', y, z, t) = p_{hi}(t)x + q_{hi}(t) \quad (13)$$

which means that, in practice, one can use the same coefficients for linear expansion of both, the densities η_e , η_h and of the functions B_e , B_h .

We introduce also the $x_{e0}(t)$ and $x_{eN}(t)$ coordinates, which denote the beginning and end of the $B_e(x, t)$ distributions for electrons. Similar coordinates $x_{h0}(t)$ and $x_{hN}(t)$ are introduced for holes (see right-upper panel in Fig. 2).

2.1. Electric field determination

In order to determine the drift velocity associated with the centers of Gaussians G_e , G_h we have to calculate the respective effective electric field acting on the carriers described by above distributions. Such a field is determined by a static voltage applied to the detector electrodes and by the Coulomb interaction between the Gaussian charge clouds. The detector static field at

position x , considered from the rear side of the detector (order $n-p$ from the point of view of the particle entering the detector, see e.g. Ref. [11]), is given as

$$E_{stat}(x) = \frac{2V_d x}{d_{Si}^2} + \frac{V - V_d}{d_{Si}} \quad (14)$$

where the bias voltage V is assumed to be higher than the depletion voltage V_d which for the bulk concentration of donors N_D and permittivity $\epsilon = \epsilon_r \epsilon_0$ reads as

$$V_d = \frac{q_0 N_D d^2}{2\epsilon_r \epsilon_0} \quad (15)$$

where q_0 is the electron charge.

In order to find the modification of the electric field caused by the generated plasma, let us consider two Gaussians describing the distribution of the charges Z_1, Z_2 , centered at a relative distance $r_{12} = |\mathbf{r}_{01} - \mathbf{r}_{02}|$ and characterized by variances σ_1^2, σ_2^2 , respectively. The mutual interaction potential of the clouds can then be expressed in the form which can be often found in quantum molecular dynamics calculations (see e.g. Ref. [13])

$$\begin{aligned} v(r_{01}, r_{02}, \sigma_1, \sigma_2) &= \frac{e^2 Z_1 Z_2}{(2\pi\sigma_1\sigma_2)^3} \iint \frac{\exp\left(-\frac{(\mathbf{r}_1 - \mathbf{r}_{01})^2}{2\sigma_1^2}\right) \exp\left(-\frac{(\mathbf{r}_2 - \mathbf{r}_{02})^2}{2\sigma_2^2}\right)}{|\mathbf{r}_1 - \mathbf{r}_2|} d^3\mathbf{r}_1 d^3\mathbf{r}_2 \\ &= e^2 Z_1 Z_2 \frac{\text{erf}\left(\frac{r_{12}}{\sqrt{2}\sigma}\right)}{r_{12}} \end{aligned} \quad (16)$$

where $\sigma = \sqrt{\sigma_1^2 + \sigma_2^2}$ and in our consideration we take $e^2 = 1.44 \times 10^{-3}$ eV μm in order to get the electrical field in V/ μm .

Let us now assume that the intervals Δx_i are small enough to enable the linear approximation for the charge densities ρ_e, ρ_h and the functions B_e, B_h with the use of the coefficients p and q . For simplicity, we introduce variables p, q in lieu of the $p_{ei}(t), p_{hi}(t)$ and $q_{ei}(t), q_{hi}(t)$. If we denote the endpoints of the Δx_i interval by c and d then for a Gaussian centered at a point a and representing the charge Z_a , its interaction with the charge located in the interval $\Delta x_i = (c, d)$ given by Eqs. (12) and (13), can be formulated as

$$V_C(a, c, d, p, q, \sigma_a, \sigma_i) = \frac{e^2}{\epsilon} Z_a \int_c^d dx (px + q) \frac{\text{erf}\left(\frac{|x-a|}{\sqrt{2}\sigma_s}\right)}{|x-a|} \quad (17)$$

where the σ_a and σ_i above denote the standard deviations of the Gaussian describing the charge Z_a and of the Gaussian from the interval Δx_i , respectively, and $\sigma_s = \sqrt{\sigma_a^2 + \sigma_i^2}$.

The above form allows us to describe the respective effective electric field E_x acting on the Gaussian located at a point a as

$$E_x(a, c, d, p, q, \sigma_a, \sigma_i) = -\frac{1}{Z_a} \frac{\partial V_C}{\partial a} = -\frac{e^2}{\epsilon} \int_c^d dx (px + q) \frac{\partial}{\partial a} \frac{\text{erf}\left(\frac{|x-a|}{\sqrt{2}\sigma_s}\right)}{|x-a|}. \quad (18)$$

Since $\partial/\partial a = -\partial/\partial x$, the above formula can be expressed as

$$\begin{aligned} E_x(a, c, d, p, q, \sigma_a, \sigma_i) &= \frac{e^2}{\epsilon} \int_c^d dx (px + q) \frac{\partial}{\partial x} \frac{\text{erf}\left(\frac{|x-a|}{\sqrt{2}\sigma_s}\right)}{|x-a|} \\ &= \frac{e^2}{\epsilon} q \left(\frac{\text{erf}\left(\frac{|d-a|}{\sqrt{2}\sigma_s}\right)}{|d-a|} - \frac{\text{erf}\left(\frac{|c-a|}{\sqrt{2}\sigma_s}\right)}{|c-a|} \right) + \frac{e^2}{\epsilon} p \int_c^d dx x \frac{\partial}{\partial x} \frac{\text{erf}\left(\frac{|x-a|}{\sqrt{2}\sigma_s}\right)}{|x-a|}. \end{aligned} \quad (19)$$

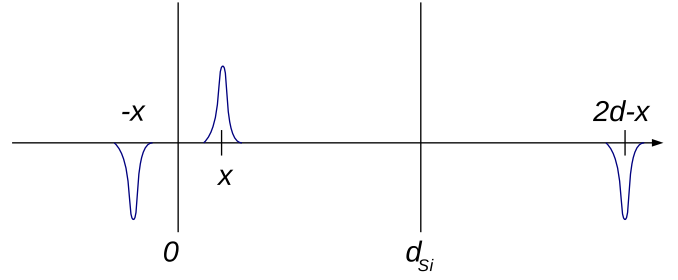


Fig. 1. Allowing the charge induced by plasma in the detector electrodes. In the present approximation we consider only the nearest mirror reflections. So the influence of the charge induced in an electrode positioned at 0 on the detector electric field acts as a part of the Gaussian localized in position $-x$ with the reverse charge and with the same variance. Similarly, the charge induced in the second electrode is represented by a respective Gaussian localized in a symmetric point at $2d_{Si}-x$.

After integrating by parts one obtains

$$\begin{aligned} E_x &= \frac{e^2}{\epsilon} q \left(\frac{\text{erf}\left(\frac{|d-a|}{\sqrt{2}\sigma_s}\right)}{|d-a|} - \frac{\text{erf}\left(\frac{|c-a|}{\sqrt{2}\sigma_s}\right)}{|c-a|} \right) \\ &+ \frac{e^2}{\epsilon} p \left(d \frac{\text{erf}\left(\frac{|d-a|}{\sqrt{2}\sigma_s}\right)}{|d-a|} - c \frac{\text{erf}\left(\frac{|c-a|}{\sqrt{2}\sigma_s}\right)}{|c-a|} \right) + \frac{e^2}{\epsilon} p \int_c^d dx \frac{\text{erf}\left(\frac{|x-a|}{\sqrt{2}\sigma_s}\right)}{|x-a|}. \end{aligned} \quad (20)$$

The last integral can be easily evaluated by expanding the error function.

The total effective electric field modified due to the presence of plasma can be obtained by summing up contributions of charges located in all intervals (c_i, d_i) and of their mirror charges induced in the detector electrodes (see Fig. 1).

In order to determine the time evolution of the charge distribution one has to know, in addition, the generalized force associated with the σ_a variable. Similarly as for the effective electric field, the net value of the force acting in the σ_a direction can be obtained by summing over all ingredients associated with the charge distribution. This leads to the following expression for the interaction with the charge located in the Δx_i interval:

$$\begin{aligned} F_{\sigma_a, a, cd} &= -\frac{\partial V_C}{\partial \sigma_a} = -\frac{e^2}{\epsilon} Z_a \int_c^d dx (px + q) \frac{\partial}{\partial \sigma_a} \frac{\text{erf}\left(\frac{|x-a|}{\sqrt{2}\sigma_s}\right)}{|x-a|} \\ &= -Z_a \frac{e^2 p \sigma_a}{\sqrt{2}\epsilon \sigma_s} \left(\exp\left(-\frac{(a-d)^2}{2\sigma_s^2}\right) - \exp\left(-\frac{(a-c)^2}{2\sigma_s^2}\right) \right) \\ &+ Z_a \frac{e^2 \sigma_a (ap + q)}{\epsilon \sigma_s^2} \left(\text{erf}\left(\frac{(a-d)}{\sqrt{2}\sigma_s}\right) - \text{erf}\left(\frac{(a-c)}{\sqrt{2}\sigma_s}\right) \right). \end{aligned} \quad (21)$$

Now we are in a position to calculate the time evolution of the charge generated in the detector. This process is determined by the drift and by the diffusion of the interacting clouds of electrons and holes. We will consider the evolution of the centroids and of the variances of Gaussians representing a fraction of the charge distribution located in the middle of the intervals Δx_i and at the start- and end-points of the distributions of electrons and holes (points $x_{e0}(t), x_{eN}(t)$ and $x_{h0}(t), x_{hN}(t)$).

2.2. Evolution of the function B

In the present subsection we will describe the numerical method used to determine the time evolution of the ionization clouds. In the following we assume that the evolution of the

functions B_e , B_h is determined by the time evolutions of the coefficients p_{ei} , q_{ei} and p_{hi} , q_{hi} . In order to find how the expansion coefficients p_{ei} , q_{ei} and p_{hi} , q_{hi} propagate in time, we have to investigate the time evolution of the functions $\eta_e(x,t)$ and $\eta_h(x,t)$ when the drift velocity of electrons and holes at the point x are, respectively, $v_{xe}(x,t)$ and $v_{xh}(x,t)$.

Below we consider the formulas for electrons only, keeping in mind that the formulas for holes are analogical.

As we will show later

$$\frac{\partial}{\partial t} \eta_e(x,t) = -\frac{\partial}{\partial x} (\eta_e(x,t) v_{xe}(x,t)) \quad (22)$$

thus, the differential $d\eta_e(x,t)$ can be written as

$$d\eta_e(x,t) = -\left(v_{xei}(x,t) \frac{\partial}{\partial x} \eta_e(x,t) + \eta_e(x,t) \frac{\partial}{\partial x} v_{xe}(x,t) \right) dt. \quad (23)$$

If the x_i denotes the center of the interval Δx_i and q_{ei} and p_{ei} are the coefficients of linear expansion

$$\eta_e(x,t) = p_{ei}(t)(x-x_i) + q_{ei} \quad (24)$$

and, if one denotes the average velocity and the average linear density associated with the interval Δx_i by $v_{xei}(t)$ and $\eta_{xei}(t)$, respectively, then

$$d\eta_{ei}(t) = -(v_{xei}(t) p_{ei}(t) + \eta_{ei}(t) \varphi_{xei}(t)) dt. \quad (25)$$

Here, $\varphi_{xei}(t)$ is the differential coefficient of $v_{xei}(x,t)$ at the point x_i . As one can see, in order to calculate the above increment, we have to trace the time dependent tables of $\eta_{ei}(t)$, $v_{xei}(t)$. The tables of $p_{ei}(t)$, $q_{ei}(t)$ and $\varphi_{xei}(t)$ are obtained by fitting the smooth curves to the distributions $\eta_{ei}(t)$, $v_{xei}(t)$ in every time step. For $t=0$ the $\eta_{ei}(t=0)$ is given by the Bragg curve. In order to make use of the formula (25) we need to construct the respective tables for velocities. Knowing the effective electric field for electrons in the x direction, E_{xei} , one can assume that the respective average velocity of the center of Gaussian located at a point x_i is proportional to the strength of the field

$$v_{xei} = \mu_{xe} E_{xei} \quad (26)$$

where μ_{xe} and μ_{xh} are the electron and hole mobilities, respectively.

Knowing the drift velocity, one can calculate the evolution of the charge deposited in every interval Δx_i including the edge intervals with variable ends $x_{e0}(t)$, $x_{en}(t)$ and $x_{h0}(t)$, $x_{hn}(t)$.

2.3. Charge propagation in the perpendicular direction

The diffusion and transport processes in the electric field influence also the widths of the charge distributions located in every Δx_i interval. Extending the above reasoning we can assume that the velocity, $v_{\sigma ei}$, describing the rate of the standard deviation expansion in perpendicular direction has three components

$$v_{\sigma ei} = v_{\sigma ei}^E + v_{\sigma ei}^D + v_{\sigma ei}^T. \quad (27)$$

The first term, $v_{\sigma ei}^E$, results from the field described by Eq. (21). In analogy to the charge drift in x direction, one can assume that this component is proportional to the field acting on the charge Z_a associated with the Gaussian with a standard deviation σ_a

$$E_{\sigma ei} = \frac{F_{\sigma a}}{Z_a} \quad (28)$$

where $F_{\sigma a}$ is the net force given by interaction (21). Thus, the respective velocity can be expressed as

$$v_{\sigma ei}^E = \mu_{\sigma e} E_{\sigma ei} \quad (29)$$

where the $\mu_{\sigma e}$ parameter is the only free parameter of the model. It seems, however, that it can be determined theoretically in the

future. A similar parameter for description of the hole propagation can be calculated assuming the following proportion:

$$\frac{\mu_{\sigma e}}{\mu_{\sigma h}} = \frac{\mu_{xe}}{\mu_{xh}}. \quad (30)$$

The velocity $v_{\sigma ei}^D$ follows from the solution of the second Fick's law for diffusions of Gaussian density distributions

$$v_{\sigma ei}^D = \frac{\partial \sigma_{ei}}{\partial t} \Big|_{v_{\sigma ei}^E = 0, v_{\sigma ei}^T = 0} = \frac{D_e}{\sigma_{ei}} \quad (31)$$

where D_e is the diffusion coefficient for electrons.

Another process which affects, on an average, the widths of the respective Gaussian distributions used to describe the charge located in the interval Δx_i , is related to the transport of the carriers. In order to describe this process we consider an increase of the variance, σ^2 , of the Gaussian distribution of the charge of Z particles contained in an interval Δx , with linear density $\eta(x) = Z/\Delta x$. Let the $\sum r_i^2$ denote the sum of squares of deviations of particle positions from the average. In this consideration we neglect the influence of the diffusion and of mutual interactions of clouds on the propagation of the variance.

The change of $\sigma^2 \equiv \sum r_i^2/Z$, resulting from the flow of particles into and out of the cell Δx (with the net value of dZ) is, in general, equal to

$$d\sigma^2 = \frac{d(\sum r_i^2)}{Z} - \frac{\sigma^2(x) dZ}{Z}. \quad (32)$$

As one can see, in order to find the increment $d\sigma^2$ we have to find the increments dZ and $d(\sum r_i^2)$.

Let us begin with the description of $d(\sum r_i^2)$. If the accretion of particles in an interval Δx across the points $x_1 = x - \Delta x/2$ and $x_2 = x + \Delta x/2$ is denoted by dZ_1 and dZ_2 , respectively, and the variances at these points are denoted by $\sigma_1^2 = \sigma^2(x - \Delta x/2)$ and $\sigma_2^2 = \sigma^2(x + \Delta x/2)$, respectively, then the increment of the sum $\sum r_i^2$ can be determined as

$$d(\sum r_i^2) = \sigma_1^2 dZ_1 - \sigma_2^2 dZ_1. \quad (33)$$

Denoting the velocities of particles at points x_1 and x_2 by $v(x - \Delta x/2)$ and $v(x + \Delta x/2)$, respectively, the accretions dZ_1 and dZ_2 can be determined as

$$dZ_1 = \eta(x - \Delta x/2) v(x - \Delta x/2) dt \quad (34)$$

$$dZ_2 = \eta(x + \Delta x/2) v(x + \Delta x/2) dt. \quad (35)$$

Now one can calculate the increment $d(\sum r_i^2)$ as

$$d(\sum r_i^2) = -dt \cdot \Delta x \cdot \left[\frac{\sigma^2(x + \Delta x/2) \eta(x + \Delta x/2) v(x + \Delta x/2) - \sigma^2(x - \Delta x/2) \eta(x - \Delta x/2) v(x - \Delta x/2)}{\Delta x} \right]. \quad (36)$$

The expression in square brackets tends to the partial derivate $(\partial(\sigma^2(x)\eta(x)v(x)))/\partial x$ for $\Delta x \rightarrow 0$.

Similarly, the increment $dZ = dZ_1 - dZ_2$ can be written as

$$dZ = -\Delta x \left[\frac{\eta(x + \Delta x/2) v(x + \Delta x/2) - \eta(x - \Delta x/2) v(x - \Delta x/2)}{\Delta x} \right] dt \quad (37)$$

and again, in the limit of $\Delta x \rightarrow 0$ the expression in square brackets approaches to $(\partial(\eta(x)v(x)))/\partial x$, which has already been used in Ref. (22).

Taking the above into account, setting $Z = \eta(x)\Delta x$ and taking the $\Delta x \rightarrow 0$ limit, Eq. (32) can be transformed into

$$d\sigma^2(x) = \left[\frac{-\partial(\sigma^2(x)\eta(x)v(x))}{\partial x} + \frac{\sigma^2(x)\partial(\eta(x)v(x))}{\partial x} \right] \frac{dt}{\eta(x)} = \frac{-v(x)\partial(\sigma^2(x))}{\partial x} dt \quad (38)$$

what gives

$$\frac{\partial \sigma^2}{\partial t} = -v \frac{\partial \sigma^2}{\partial x} \Rightarrow \frac{\partial \sigma}{\partial t} = -v \frac{\partial \sigma}{\partial x}. \quad (39)$$

Finally for $v_{\sigma_{ei}}^E = 0$ and $v_{\sigma_{ei}}^D = 0$ one can write

$$v_{\sigma_{ei}}^T = \left. \frac{\partial \sigma_{ei}}{\partial t} \right|_{v_{\sigma_{ei}}^E = 0, v_{\sigma_{ei}}^D = 0} = -v_{xei} \frac{\partial \sigma_{ei}}{\partial x}. \quad (40)$$

In order to use the above formula we trace the changes of the vector of σ_{ei} values as a function of the position index, i . Knowledge of velocities $v_{\sigma_{ei}}^E$, $v_{\sigma_{ei}}^D$ and $v_{\sigma_{ei}}^T$ allows to calculate the propagation of the width of the distribution of electrons. The formulas for holes are analogical.

3. First prediction of the model and comparison with the experimental data

For the first comparison of the model prediction with the experimental data we choose the data for ^{12}C ion which have already been used in Ref. [11]. This gives also the opportunity to compare the present model predictions with those obtained in a more phenomenological approach. For the measurement the neutron transmutation doped (n-TD) silicon detector [14] was used. This n-type bulk and extremely thin p-type zone has a thickness $d_{Si} = 310 \mu\text{m}$ (resistivity 2.5 k Ω cm; depletion bias 128 V and operation bias 190 V). The energy measurement was performed using the charge output, while the current pulses were measured using the current output of the same preamplifier, described in Ref. [9] (for acquisition large bandwidth digital oscilloscope with sensitivity 5 mV/div for incident energy 80 MeV). This paper presents also in detail the experimental setup and conditions used for the ^{12}C ions (and LCP).

Before describing the induced current pulse, we focus first on the propagation of the electric field and the propagation of the electron and hole densities in parallel and perpendicular directions. The evolution of these observables is important for understanding the mechanism of the plasma delay process. In the following, we consider an ^{12}C ion impinging on the n-type rear side of the silicon detector. This, so called “rear-mount”, gives quite different shapes as compared to the “standard mount”, and these pulse shapes are much better suited for the PSD technique [9].

For actual calculations it is necessary to set some physical coefficients describing the electric field propagation, as well as coefficients describing the drift and diffusion process in silicon. In Table 1 we collect values of these parameters:

It should be emphasized that the adoption of a fixed value of mobility represents a significant approximation. In general, the electron and holes mobilities depend on the donor and acceptor concentrations, impurity concentrations, defect concentration and electron and hole concentrations. It also depends on the temperature and electric field, and usually is determined empirically.

For small values of the electric field (under 1 kV/cm at temperature 300 K) mobility remains approximately constant. With increasing field value it tends to saturation and reaches maximum value depending on the doping values [15]. In our case the electric field reaches the value of 6 kV/cm, which suggests that in the future the mobility needs to be more precisely determined as a field strength function (and other parameters). It will be done in the forthcoming paper.

As already mentioned, the electric field propagation results from the static detector bias and from the generated charge density propagation. At the starting point, when the generated electrons and holes are almost exactly at the same positions, the electric field is still equal to the external one (14). This field, for

Table 1
Model Parameters

Feature	Symbol	Value	Remarks
Energy per e–h pair creation	w	3.6 $\left(\frac{\text{eV}}{\text{pair}}\right)$	Material constant
Silicon dielectric, permittivity	ϵ_r	11.7	Material constant
Electrons mobility	μ_{xe}	135 $\left(\frac{\mu\text{m}^2}{\text{Vns}}\right)$	Material constant
Holes mobility	μ_{xh}	47.5 $\left(\frac{\mu\text{m}^2}{\text{Vns}}\right)$	Material constant
Electrons variance mobility	$\mu_{\sigma e}$	2 $\left(\frac{\mu\text{m}^2}{\text{Vns}}\right)$	Free parameter
Holes variance mobility	$\mu_{\sigma h}$	$\mu_{\sigma h} = \mu_{\sigma e} \frac{\mu_{xh}}{\mu_{xe}}$	Model assumption
Diffusion coefficient for electrons	D_e	3.49 $\left(\frac{\mu\text{m}^2}{\text{ns}}\right)$	Material constant
Diffusion coefficient for holes	D_h	1.228 $\left(\frac{\mu\text{m}^2}{\text{ns}}\right)$	Material constant

$t=0$, is denoted in Fig. 2 by a dotted line. After this initial moment the static field causes the shift of the electron and hole distributions and therefore in the next moment some of the carriers are moved outside of the overlap region. Next, the variance of the Gaussian partial density distribution associated with these carriers begins to grow, due to the non-compensated electric field in perpendicular direction. This effect, which is displayed in Fig. 3, causes breaking of the initial bonds between the electrons and holes. As a result, the considered electrons and holes start leaking slowly from the overlap region and begin moving in opposite directions. At the same time, the increasing shift between electrons and holes leads to significant reduction of the electric field in the interaction region. This scenario is well associated with the postulates of the phenomenological model of Ref. [11].

The evolution of the charge density, the effective electric field and the variances of the Gaussian partial densities are presented in Figs. 2–5 in which the dashed blue lines represent the dependences for the electrons while the dotted red ones represent the holes. Fig. 2 shows the evolution of the linear electron and hole densities. One can see that, during the first 20–30 ns, the electrons and holes remain bound in the region close to the detector surface. After that time, one can observe the electric field restitution practically in the whole detector area. The time behavior of the electric field is presented in Fig. 3. In order to save the calculation time, the field is calculated only at points where the density of the particles is not equal to zero. Fig. 4 presents the evolution of the width of the charge distributions. We can notice that in the overlap region the effective electric field is reduced to very low value. As one can see, the evolutions of the electric field and of the charge densities (in parallel and perpendicular directions) are strongly correlated.

Up to now, the mutual Coulomb interactions between the charge clouds have been taken into account. In order to see the importance of these mutual interactions, they have been neglected in the charge density evolutions presented in Fig. 5. As one can see, in this case (no field screening by the charge clouds), the collection time becomes about three times shorter.

Knowledge of the charge propagation, by using of the Ramo–Shockley theorem [16–18], allowed as to determine the current pulse time dependence. Speed of all charges Q_i which can impact on the induced charge in detector electrodes is required. According to Ramo–Shockley theorem thesis, the partial current induced by moving, electrical charge Q_i in the k th electrode is equal to

$$i_k(Q_i, \mathbf{v}_i, \psi_k) = Q_i \mathbf{v}_i \cdot \psi_k \quad (41)$$

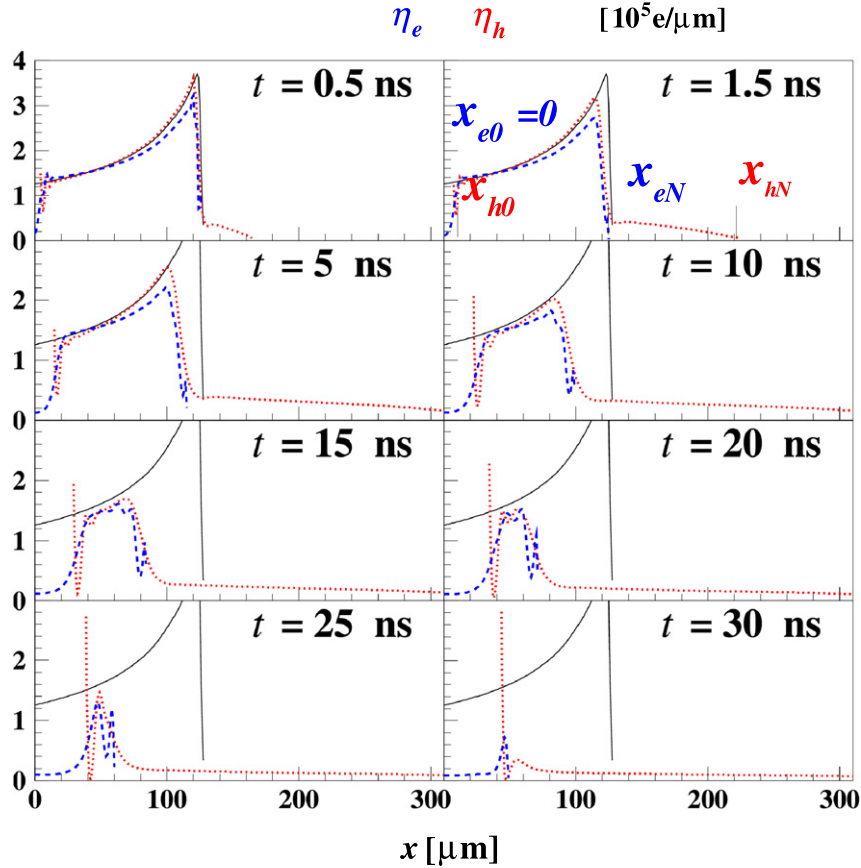


Fig. 2. Propagation of the linear density of the electrons η_e (dashed blue lines) and the holes η_h (dotted red lines) due to the ionization induced by 80 MeV ^{12}C ion entering the Si detector from the rear side. (For interpretation of the references to color in this figure legend, the reader is referred to the web version of this article.)

where vector \mathbf{v}_i is the velocity of charge Q_i , and ψ_k is a vector (weighting field - space constant) which is defined as electrical field in following conditions:

1. All electrical charges are removed from the detector space.
2. Potential of k th electrode is set to 1 V and for all other electrodes the potentials are set to zero.

The total induced current is the sum of all currents involved.

In order to obtain a rough estimate of the pulse shape, we describe the partial current associated with the Gaussian cloud in approximate way. For simplification, using Ramo–Shockley theorem, we replace the Gaussian charge distribution by a point-like one. Such an approach neglects effects associated with the charge diffuseness, particularly for clouds moving closely to the detector electrodes.

The result of such a calculation is presented in Fig. 6. The total current pulse is denoted by black solid line while the electron and hole contributions are represented by the dashed blue and dotted red ones, respectively.

For comparison of the calculated pulse with the experimental one the primary pulses from Fig. 6. have been corrected (see Ref. [3]) for the preamplifier's response. The results are shown in Fig. 7. We have to stress that in the present calculations we did not search for the best value of the $\mu_{\sigma e}$ parameter. We also did not consider some quite complicated factors, specified below, which could affect the obtained results and which will be a subject of the forthcoming paper:

- (i) precision of the Energy-Range tables (average accuracy of about 10%, see Ref. [12]),

- (ii) diffuseness of the Gaussian clouds and its presence in the application of the Ramo–Shockley theorem,
- (iii) dead layers of the detector (in the present case, at low field region, it might be an $n-n^+$ contact) and their effect on the converted to the charge energy (as one can see in Fig. 8, for 80 MeV ^{12}C the collection time is very sensitive on the ion energy),
- (iv) accuracy of the active detector thickness and of the electric field determination,
- (v) accuracy of the preamplifier response description.

According to significant impact of v point on the results, below we will develop a bit more about it. The charge sensitive preamplifier, as a FRONT-END electronic system, is directly coupled to the detector, and participates in the signal reception. Therefore, the resulting pulse is under strong influence of the preamplifier parameters, particularly the cutoff frequency ω_0 (frequency at which the op amp gain is equal to 1, also known as a unity gain frequency). These parameters are mainly determined by the parameters of transistors, but they also depend on the geometry of an electronic circuit (assembly capacitance). The response of the preamplifier electronics to the input current pulse (e.g. resulting from the presented calculations) can be simulated using a dedicated software (for instance, the one mentioned in Ref. [9]). However, due to the fundamental importance of the pulse rise time for the particle identification procedure, we would like to briefly discuss the conditions that determine the rise time.

The amplifier with closed feedback loop, amplifying a voltage signal, has the upper bandwidth frequencies given by a well-known

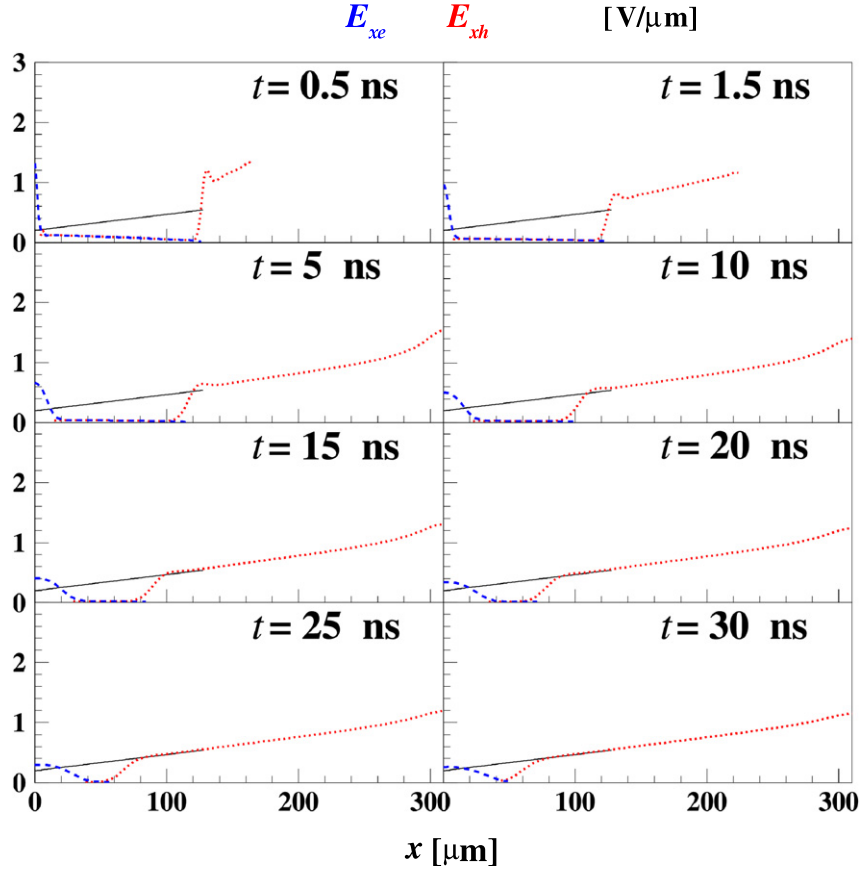


Fig. 3. The effective electric field strength inside the silicon detector at different moments in time, due to the ionization induced by 80 MeV ^{12}C ion penetrating the detector from the rear side. The solid line gives the undisturbed electric field for $t=0$. The field is calculated only at points with coordinate x where the density of electrons (dashed blue line) and holes (dotted red line) is not equal to zero. (For interpretation of the references to color in this figure legend, the reader is referred to the web version of this article.)

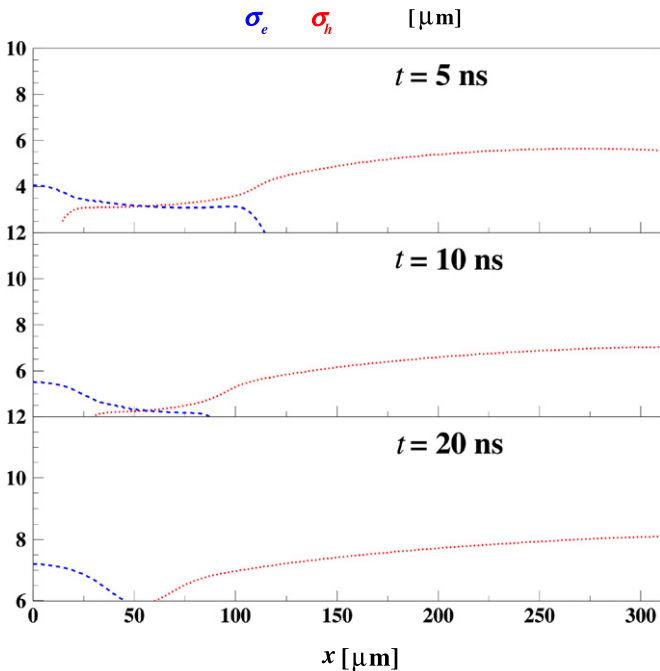


Fig. 4. Time evolution of the width of the charge distribution which determines the charge propagation in the perpendicular direction. Standard deviations for electrons are represented by the dashed blue line and variances for the holes by the dotted red one. (For interpretation of the references to color in this figure legend, the reader is referred to the web version of this article.)

formula

$$\omega_C = \frac{\omega_0}{K_u} \quad (42)$$

where K_u is the gain of the amplifier. It is so because, for operational amplifier, the gain–bandwidth product $K_u\omega_C$ is nearly independent of the gain K_u at which it is measured. Knowing the upper frequency of this band we can determine the intrinsic preamplifier rise time as

$$\tau_{preamp} = \frac{1}{\omega_C}. \quad (43)$$

For the harmonics signals, the gain K_u can be calculated as follows:

$$K_u = 1 + \frac{Z_f}{Z_{in}} \approx \frac{C_D}{C_f}, \quad C_D \gg C_f \quad (44)$$

where Z_f is the feedback impedance (in our case it is the impedance of a small capacity C_f (~ 1 pF)) and Z_{in} is the impedance connected to the amplifier input (here it is approximately determined by the detector capacity C_D , we skip the small pre-amp input capacitance and high resistance of the input, see Fig. 9). Now, the intrinsic preamplifier rise time is given by the formula

$$\tau_{preamp} \approx \frac{C_D}{\omega_0 C_f} \quad (45)$$

In the present approximate one can see that the preamplifier rise time is proportional to the detector capacitance. This is so because the increase of the detector capacity increases the voltage

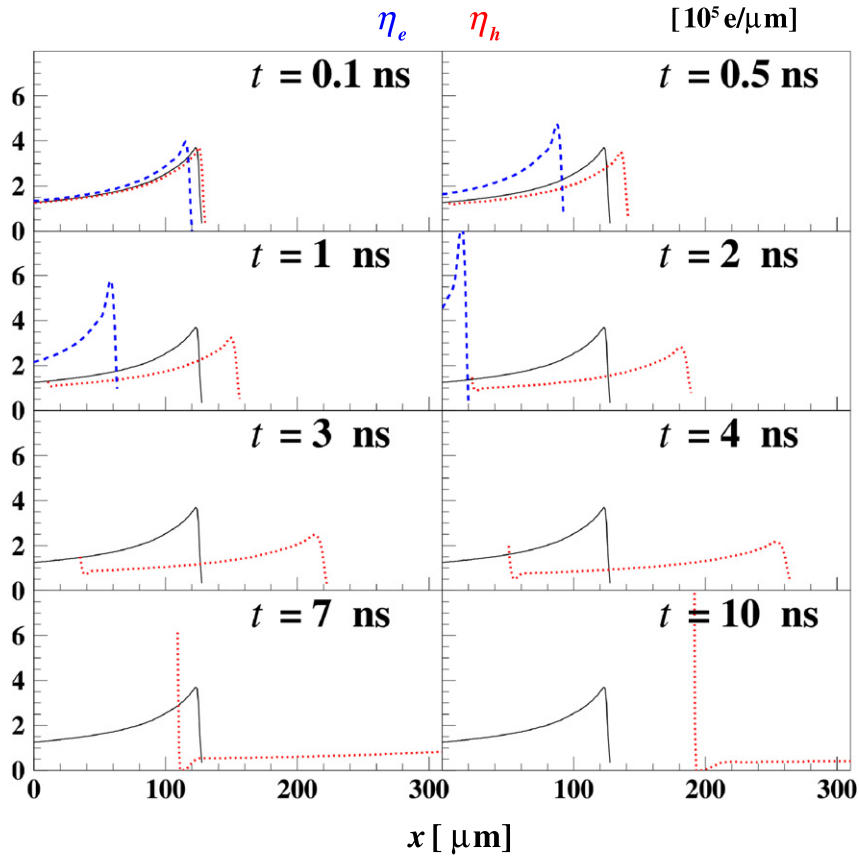


Fig. 5. Same as Fig. 2, but neglecting the mutual Coulomb interactions between the carrier clouds. Significant difference in the charge collection time can be observed as compared to the complete case (see Fig. 2). (For interpretation of the references to color in this figure legend, the reader is referred to the web version of this article.)

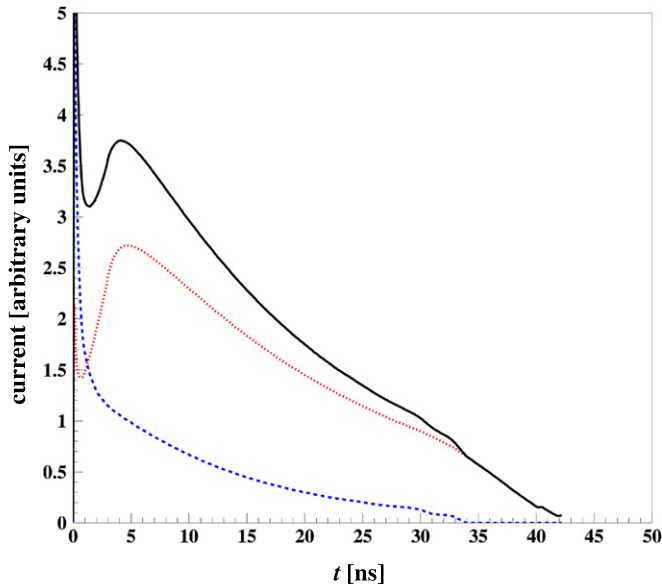


Fig. 6. Model prediction of the current signal induced by an 80 MeV ^{12}C ion penetrating the silicon detector from the rear side. The predictions are not corrected for the preamplifier response. The solid, black line represents the total signal, the dashed blue line presents the electron contribution while the dotted red one the hole contribution. (For interpretation of the references to color in this figure legend, the reader is referred to the web version of this article.)

gain what consequently reduces the bandwidth. The behavior of the rise time, presented in Ref. [19] in Fig. 2 is qualitatively consistent with that described above. In the case of high value of the capacitance C_D the total pulse rise time can be determined

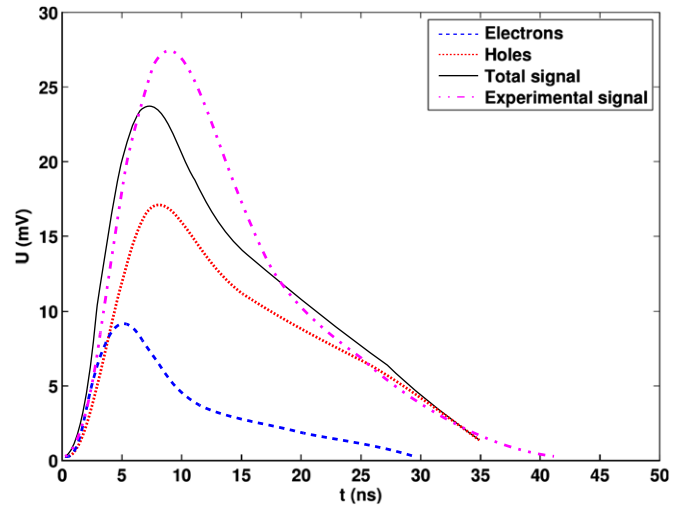


Fig. 7. Same as Fig. 6 but the respective lines have been corrected for the preamplifier's response.

by τ_{preamp} . In the case we studied the preamplifier rise time seems to be a bit longer than 5 ns.

In order to demonstrate that the present model is able to describe correctly the plasma delay effect. In Fig. 8, we present the correlation between the collection time and the energy loss for ^{10}B , ^{12}C , and ^{14}N ions. We use the collection time rather than the experimentally preferred rise time, noting that these two observables are strongly correlated. Fig. 8 shows that the model can reproduce the experimental trends, especially the characteristic “back-bending” of identification curves at low energies.

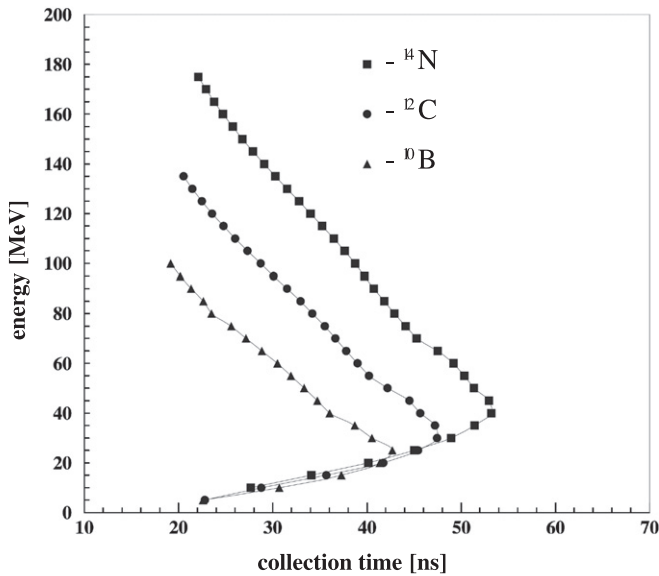


Fig. 8. Model prediction for correlations: energy vs collection time.

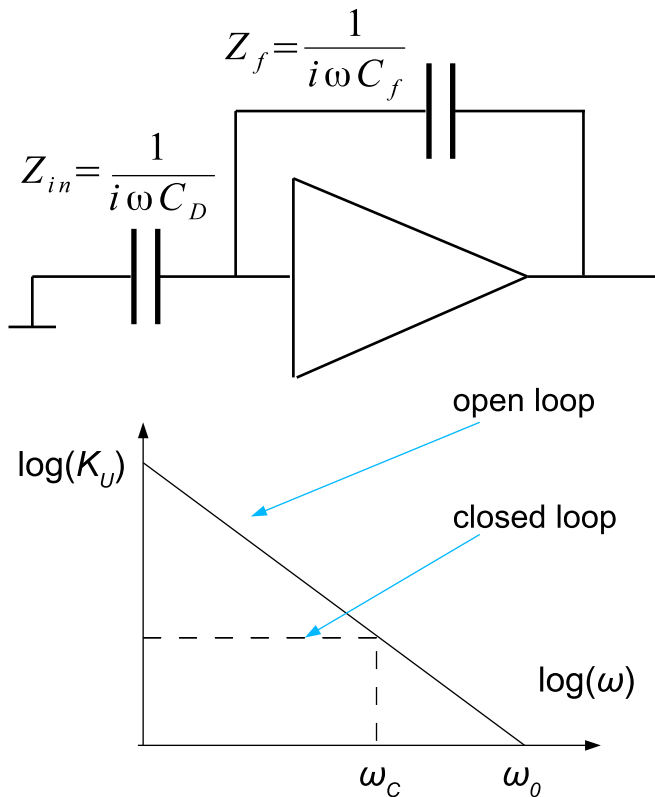


Fig. 9. Influence of the feedback capacitance and detector capacitance on the preamplifier rise time. (For interpretation of the references to color in this figure legend, the reader is referred to the web version of this article.)

4. Conclusions

We have proposed a description of the evolution of charge density and of the effective electric field by taking into account the mutual Coulomb interactions between the charge carrier distributions. According to the present approach the plasma delay effect is associated with the propagation of the carriers in both directions, perpendicular and parallel to the primary ionization path.

The duration of the obtained pulse for the 80 MeV ^{12}C ion, corresponds quite well to the one obtained in the physical measurement. Also the shape of the energy-collection time correlation and its element dependence are quite well reproduced by the model. Nevertheless, the model still needs to be confronted with a broader collection of the experimental data obtained for detectors of various thicknesses and biased by various voltages.

Once tested on a broader collection of the experimental pulse shapes, the model will enable the theoretical search for the best identification method based on the pulse shape analysis. It will also enable the study of the dependence of the identification quality on the detector thickness and maybe on some special construction of the detector with non-linear electric field (obtained by the heterogeneity of doping) for regions with poor resolution (small ion energy, see Fig. 8). The presented approach should be also suitable for testing the temperature dependence (via the respective dependence of the diffusion coefficients).

In order to draw some more quantitative conclusions from the comparison of the model with the experimental data one has to estimate the uncertainties related to various possible ingredients, mentioned in the previous paragraph. Also we have to make an attempt to constrain the single free parameter μ_{se} from the respective classical consideration.

The actual model calculation is quite time consuming. For standard processor the calculation of one pulse associated with the 80 MeV ^{12}C ion, takes about 5 h of CPU, thus some code optimization is still needed.

Acknowledgment

The author is indebted to J. Łukasik and P. Kulig for their careful reading of the manuscript and helpful discussions. Special thanks for H. Hamrita for his calculations of the preamplifier response.

Work supported by Polish Ministry of Science and Higher Education under Grant no. DPN/N108/GSI/2009.

References

- [1] C.A. Ammerlaan, et al., Nuclear Instruments and Methods 22 (1963) 189.
- [2] W. Seibt, et al., Nuclear Instruments and Methods 113 (1973) 317.
- [3] P.A. Tove, W. Seibt, W. Leitz, Nuclear Instruments and Methods 51 (1967) 304.
- [4] A.A. Quaranta, A. Taroni, G. Zanarini, IEEE Transactions on Nuclear Science NS-15 (1968) 373.
- [5] H.O. Neidel, H. Henschel, Nuclear Instruments and Methods 178 (1980) 137.
- [6] W. Bohne, et al., Nuclear Instruments and Methods in Physics Research Section A 240 (1985) 145.
- [7] J.B. England, G.M. Field, T.R. Ophel, Nuclear Instruments and Methods in Physics Research Section A 280 (1989) 291.
- [8] G. Paush, et al., Nuclear Instruments and Methods in Physics Research Section A 365 (1995) 176.
- [9] H. Hamrita, et al., Nuclear Instruments and Methods in Physics Research Section A 531 (2004) 607.
- [10] L. Bardelli, G. Poggi, in: R. Bougault, A. Pagano, S. Pirrone, M-F. Rivet, F. Rizzo (Eds.), Proceedings of the IWM2005, International Workshop on Multifragmentation and Related Topics, Catania, Italy, 28 November–1 December, 2005, p. 75.
- [11] M. Parlog, et al., Nuclear Instruments and Methods in Physics Research Section A 613 (2010) 290.
- [12] J.F. Ziegler, et al., The Stopping and Range of Ions in Matter (SRIM), Pergamon Press, New York, 1985.
- [13] M. Papa, et al., Physical Review C 64 (2001) 024612.
- [14] W. von Ammon, Nuclear Instruments and Methods in Physics Research Section B 63 (1992) 95.
- [15] C. Jacoboni, C. Canali, G. Ottaviani, A.A. Quaranta, Solid-State Electronics 20 (2) (1977) 77.
- [16] W. Shockley, Journal of Applied Physics 9 (1938) 635.
- [17] S. Ramo, Proceedings of the Institute of Radio Engineers 27 (1939) 584.
- [18] Hunsuk Kim, et al., Solid-State Electronics 34 (11) (1991) 1251.
- [19] H. Hamrita, et al., Nuclear Instruments and Methods in Physics Research Section A 642 (2011) 59.